

Joint Multiresolution and Background Detection Reconstruction for Magnetic Particle Imaging

Christine Droigk, Marco Maass, Corbinian Englisch, Alfred Mertins

Institute for Signal Processing, University of Lübeck
droigk@isip.uni-luebeck.de

Abstract. Magnetic particle imaging is a tracer-based medical imaging technology that is quite promising for the task of imaging vessel structures or blood flows. From this possible application it can be deduced that significant areas of the image domain are related to background, because the tracer material is only inside the vessels and not in the surrounding tissue. From this fact alone it seems promising to detect the background of the image in early stages of the reconstruction process. This paper proposes a multiresolution and segmentation based reconstruction, where the background is detected on a coarse level of the reconstruction with only few degrees of freedom by a Gaussian-mixture model and transferred to finer reconstruction levels.

1 Introduction

Magnetic particle imaging (MPI) is a tracer-based medical imaging method which was published in 2005 [1]. It is based on the nonlinear magnetization behavior of super-paramagnetic iron-oxide particles (SPIOs). The goal is to ascertain the SPIOs' distribution inside a volume, e.g. the distribution inside the vessel structure of a patient. Therefore, MPI scanners measure the induced voltage from the SPIOs' distribution by their change of magnetization. Fortunately, only SPIOs around the vicinity of the field free point (FFP) can significantly contribute to the voltage signal due to the nonlinear magnetization of those [2]. The FFP is the position where the different magnetic fields cancel each other out and this point is in MPI periodically moved, e.g. by a Lissajous trajectory, over the field of view. However, for two- and three-dimensional MPI there is no closed-form solution known so far for the system function, which relates the measured signal to the SPIOs distribution and vice versa [3]. This is the reason that the system function is normally approximated by a linear model. The resulting matrix models the spatio-temporal relationship and is called system matrix.

MPI offers a relatively high spatial and temporal resolution. To exploit the full spatial resolution, the system matrix has to be large in size. Unfortunately, solving the linear inverse problem becomes quite slow for dense system matrices. To speed up the reconstruction process, different matrix compression strategies were developed [4, 5]. The main idea is based on the usage of transforms, like the discrete cosine transform (DCT), to compress the system matrix. Recently,

a simultaneous compression and multiresolution formulation for the system matrix was proposed. The authors also presented a multiresolution reconstruction procedure based on this formulation [6].

With the new formulation of the system matrix, a level-wise background segmentation and image reconstruction is proposed. The idea to exclude regions without SPIOs inside the reconstruction is based on the work in [7]. A quite similar idea was presented in [8], but there the background information was coming from an additional magnetic resonance image scan and is used for structural prior information. For the background segmentation a Gaussian mixture model (GMM) is used, which has also been successfully applied in positron emission tomography [9]. It will be shown that the background segmentation will help to significantly improve the particle distribution reconstruction at finer resolution levels.

2 Materials and methods

2.1 Multiresolution reconstruction

Due to page limitation the description is shortened to the necessary parts of the multiresolution system matrix approach from [6]. Let $\mathbf{S}^\ell \in \mathbb{C}^{M \times K_\ell}$ be the low-resolution system matrix (low-pass approximation on the $(\ell - 1)$ -th level of the discrete wavelet transform (DWT)) with $K_\ell = \lceil \frac{N_x}{2^\ell} \rceil \cdot \lceil \frac{N_y}{2^\ell} \rceil$ where $\lceil \cdot \rceil$ denotes the ceiling operator and N_x, N_y are the numbers of pixels in x and y direction. Then the transform matrix $\mathbf{T}_\ell \in \mathbb{R}^{K_\ell \times K_\ell}$ denotes one stage of the DWT+DCT. The DWT+DCT decomposition is mathematically described by $\mathbf{S}_T^\ell = \mathbf{S}^\ell \mathbf{T}_\ell$. The level-wise particle distribution reconstruction is defined as follows

$$\mathbf{c}^\ell = \underset{\mathbf{c} \in \mathbb{R}_+^{K_\ell}}{\operatorname{argmin}} \|\mathbf{S}_T^\ell \mathbf{T}_\ell^{-1} \mathbf{c} - \mathbf{f}\|_2^2 + \lambda^2 \|\mathbf{c}\|_2^2 \quad (1)$$

where $\lambda > 0$ is the regularization factor $\mathbf{f} \in \mathbb{C}^M$ defines the measured frequency components, which are derived from the voltage signal \mathbf{T}_ℓ^{-1} is the inverse DWT+DCT and $\mathbf{c}^\ell \in \mathbb{R}_+^{K_\ell}$ denotes the unknown particle distribution on the resolution stage ℓ . Preknowledge about the background pixels can be obtained by a segmentation on the coarser level reconstruction and then transferred to the finer resolution levels. Let \mathbb{B} denote the set of background pixel indices and $\mathbb{P} = \{\mathbf{c} \in \mathbb{R}_+^{K_\ell} | \forall i \in \mathbb{B} : c_i = 0\}$ then the problem in (1) can be reformulated to the easier problem

$$\mathbf{c}^\ell = \underset{\mathbf{c} \in \mathbb{P}}{\operatorname{argmin}} \|\mathbf{S}_T^\ell \mathbf{T}_\ell^{-1} \mathbf{c} - \mathbf{f}\|_2^2 + \lambda^2 \|\mathbf{c}\|_2^2 \quad (2)$$

This problem is solved by an iterative shrinkage thresholding algorithm [10].

2.2 Background detection

To separate foreground and background pixels a thresholding with a variable threshold at each level is used. The threshold is obtained by estimating the

probability density function of the foreground and background pixels with a GMM. The obtained mask is postprocessed by some morphological operations.

It is assumed that both the reconstructed particle distribution of the background and the foreground pixels follow a Gaussian distribution. Mean, standard deviation and mixture weights are estimated by a GMM. For the approximated density follows $p(x|\boldsymbol{\theta}) = \sum_{i=1}^K \lambda_i f(x|\mu_i, \sigma_i)$, with $\boldsymbol{\theta} = (\boldsymbol{\mu}, \boldsymbol{\sigma})$ the parameter vector, $f(x|\mu, \sigma)$ the probability density function of the normal distribution with mean μ and standard deviation σ , and K the number of components. In this paper $K = 2$ is used under the assumption that contained structures share a similar concentration of the tracer. The weights λ_i can be seen as the estimation of the a-priori probability P_i . Then the threshold can be obtained by a maximum a-posteriori estimation, which is a solution of $P_1 f(x|\mu_1, \sigma_1) = P_2 f(x|\mu_2, \sigma_2)$. In the case of two solutions, the one between μ_1 and μ_2 is the desired one. Now the thresholding is performed and a binary mask is obtained. Small areas of foreground are deleted by morphological operations and then the structures are extended to preserve foreground. The obtained mask is used to set background pixels to zero during the reconstruction process. This procedure is repeated at each level and in this way the mask is refined step by step. After a successful masking the amount of background pixels that are not set to zero decreases. For this reason only concentrations $c_k > 0$ are used for the GMM estimation. Besides, if the masking is nearly perfect, there only exists a single cluster of concentration values. This results for the GMM in two means which are close together. For detection of this case, it was tested whether $2 \cdot \min(\mu_1, \mu_2) < \max(\mu_1, \mu_2)$ is satisfied. If this is not fulfilled, no further thresholding is performed at this level.

2.3 Test setup

For the simulation of the MPI scanner the Langevin model of paramagnetism was used. The simulated MPI scanner has the frequency ratio of $f_x/f_y = 32/33$ with $f_x = 25.25$ KHz for the acceleration fields. This ratio results in a Lissajous FFP-trajectory with a repetition time of 1.27 ms. For the gradient fields in both spatial directions gradients up to a strength of 1.25 Tm^{-1} were used. The simulated system matrix was sampled for both receive channels up to a frequency of 1.3 MHz, which corresponds to 2×817 frequency components for a real-valued voltage signal. For the Langevin model a particle size of 30 nm and body temperature was assumed. The field of view had a size of $5 \times 5 \text{ cm}^2$.

The multiscale segmentation reconstruction algorithm was tested on different concentration phantoms with different SNRs. In view of an application in the field of visualization of the blood flow, vessel structures were used as phantoms. Each phantom had a size of 250×250 pixels. The background had the value 0 while the concentration in the structures was 1.

For comparison purposes, also a reconstruction without foreground segmentation was performed [6], which is referred to as the baseline. A variation, where the thresholding method was used at the last level after completed reconstruction, is also included. The root mean square error (RMSE) and the structural similarity index (SSIM) [11] are used as measurements for comparison.

An RMSE near to zero shows a low difference in the concentration levels, while an SSIM near to one shows highly similar structures. A 9/7 wavelet decomposition in four levels was used.

3 Results

In Fig. 1 the ground truth concentrations and the reconstructed concentrations for an SNR of 20 dB for all compared approaches are shown. It can be observed that the proposed approach deletes background noise and delivers less blurring around the edges of the vessels than the other reconstruction results.

Fig. 2 shows the results of RMSE and SSIM for the different phantoms and methods in dependence of the SNR. The regularization parameter λ was chosen to produce the best RMSE or SSIM, respectively. It can be observed that the SSIM value of the proposed method is significantly higher for all phantoms and all SNRs than the value of the baseline. For most SNRs, advantages can be seen in comparison to the thresholded baseline method as well. The RMSE of the postprocessed baseline is better than the original baseline results for all phantoms and all SNRs. The results for the proposed method with regard to the

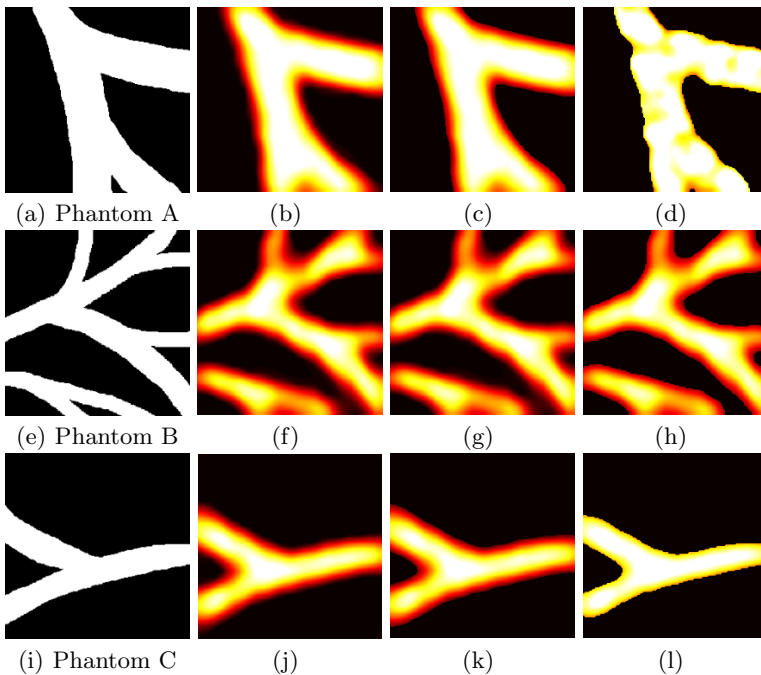


Fig. 1. Best reconstructions of the three phantoms for the tested methods and an SNR of 20 dB. The left column shows the ground truth. In the middle, the reconstructions of the baseline and the thresholded baseline are depicted. On the right the final results of the proposed method are shown.

RMSE for phantom B and C is equal or better than the other approaches. For high SNRs and for phantom A a worsening can be seen.

4 Discussion

It could be observed that the proposed method provides a reconstruction with improved SSIM compared to standard reconstruction and even to postprocessed reconstructions. It works well for different structures and improves especially the SSIM while delivering a similar RMSE in most cases. With increasing SNR the RMSE value becomes unexpectedly worse. Fig. 3 shows the estimation of the multilevel thresholded approach and the result for the baseline method. At some areas at the borders of the vessels the foreground is underestimated and as a consequence high estimations of the concentration appear at the border and lead to a high RMSE value, though in the authors' perception the quality of this estimation is better. To avoid this phenomenon, the strong enhancement at the mask boundaries could be used to detect mismasked areas and expand the mask around these edges. The enhancement of the SSIM is due to the suppression of the background noise in areas without tracer concentration and the generation of sharp edges. This disambiguates in a more homogenous concentration inside the object. Our further research is directed towards a speeding up of the reconstruction process using the obtained masks. Instead of setting the background to zero in each step, the calculations at these positions are not necessary and could be skipped. This could result in a faster reconstruction.

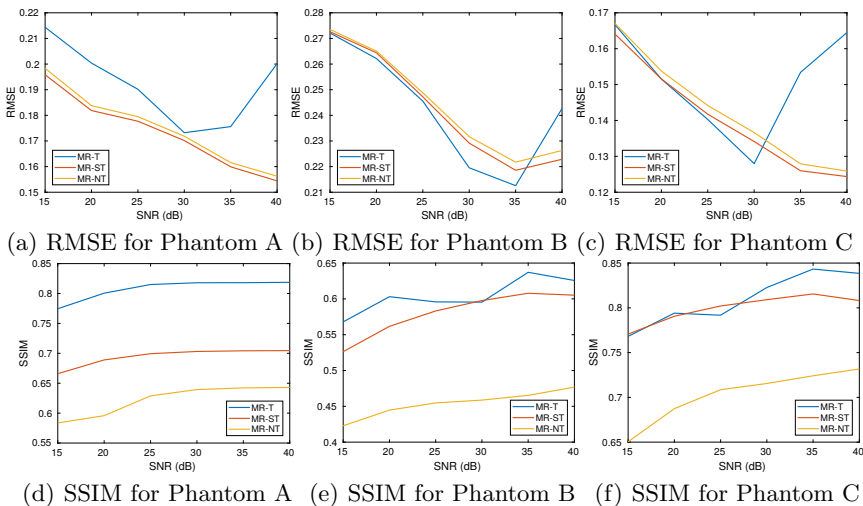
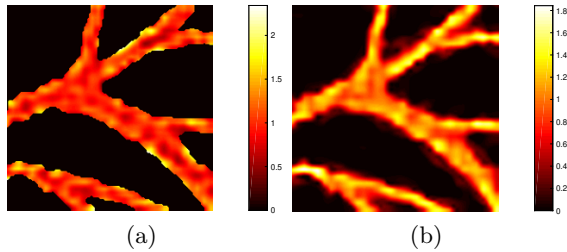


Fig. 2. RMSE and SSIM for the tested phantoms and different methods. The proposed method with foreground segmentation is referred to as MR-T, the baseline is MR-NT, and the postprocessed baseline is MR-ST. For each method and for each SNR the regularization parameter with the best result among the tested values was used.

Fig. 3. Particle distribution estimation of phantom B with an SNR of 40 dB with the proposed method (a) and the baseline system (b).



Acknowledgement. This work was supported by the German Research Foundation under grant number ME 1170/7-1.

References

1. Gleich B, Weizenecker J. Tomographic imaging using the nonlinear response of magnetic particles. *Nature*. 2005;435(7046):1214–1217.
2. Knopp T, Buzug TM. *Magnetic Particle Imaging: An Introduction to Imaging Principles and Scanner Instrumentation*. Berlin/Heidelberg: Springer; 2012.
3. Rahmer J, Weizenecker J, Gleich B, et al. Signal encoding in magnetic particle imaging: properties of the system function. *BMC Med Imaging*. 2009;9(4):4.
4. Lampe J, Bassoy C, Rahmer J, et al. Fast reconstruction in magnetic particle imaging. *Phys Med Biol*. 2012;57(4):1113–1134.
5. Knopp T, Weber A. Local system matrix compression for efficient reconstruction in magnetic particle imaging. *Adv Math Phys*. 2015;2015(Article ID 472818):1–7.
6. Maass M, Mink C, Mertins A. Joint multiresolution magnetic particle imaging and system matrix compression. *Int J Magn Part Imaging*. 2018;4(2).
7. Siebert H, Maass M, Ahlberg M, et al. MMSE MPI reconstruction using background identification. *Proc Int Workshop Magn Part Imaging*. 2016; p. 58.
8. Bathke C, Kluth T, Brandt C, et al. Improved image reconstruction in magnetic particle imaging using structural a priori information. *Int J Magn Part Imaging*. 2017;3(1).
9. Layer T, Blaickner M, Knäusl B, et al. PET image segmentation using a gaussian mixture model and markov random fields. *EJNMMI Phys*. 2015;2(1).
10. Beck A, Teboulle M. A fast iterative shrinkage-thresholding algorithm for linear inverse problems. *SIAM J Imaging Sci*. 2009;2(1):183–202.
11. Wang Z, Bovik AC, Sheikh HR, et al. Image quality assessment: from error visibility to structural similarity. *IEEE Trans Image Process*. 2004;13(4):600–612.